



PCCP

Efficiency Analysis of Helium-cooled MAS DNP: Case Studies of Surface-Modified Nanoparticles and Homogeneous Small-Molecule Solutions

Journal:	<i>Physical Chemistry Chemical Physics</i>
Manuscript ID	CP-ART-10-2020-005658.R2
Article Type:	Paper
Date Submitted by the Author:	15-Feb-2021
Complete List of Authors:	Matsuki, Yoh; Osaka University Institute for Protein Research, Kobayashi, Takeshi; U.S. DOE Ames National Laboratory, Fukazawa, Jun; Osaka University Institute for Protein Research Perras, Frédéric; US DOE Ames Laboratory, Pruski, Marek; U.S. DOE Ames Laboratory, ; Iowa State University, Department of Chemistry Fujiwara, Toshimichi; Osaka University, Institute for Protein Research

SCHOLARONE™
Manuscripts

ARTICLE

Efficiency Analysis of Helium-cooled MAS DNP: Case Studies of Surface-Modified Nanoparticles and Homogeneous Small-Molecule Solutions

Received 00th January 20xx,
Accepted 00th January 20xx

DOI: 10.1039/x0xx00000x

Yoh Matsuki,^{a,b} Takeshi Kobayashi,^{*c} Jun Fukazawa,^a Frédéric A. Perras,^c Marek Pruski,^{*c,d} and Toshimichi Fujiwara^{*a,b}

Despite the growing number of successful applications of dynamic nuclear polarization (DNP)-enhanced magic-angle spinning (MAS) NMR in structural biology and materials science, the nuclear polarizations achieved by current MAS DNP instrumentation are still considerably lower than the theoretical maximum. The method could be significantly strengthened if experiments were performed at temperatures much lower than those currently widely used (~100 K). Recently, the prospects of helium (He)-cooled DNP have been increased with the instrumental developments in MAS technology that uses cold helium gas for sample cooling. Despite the additional gains in sensitivity that have been observed with He-cooled MAS DNP, the performance of the technique has not been evaluated in the case of surfaces and interfaces that benefit the most from DNP. Herein, we studied the efficiency of DNP at temperatures between ~30 K and ~100 K for organically functionalized silica material and a homogeneous solution of small organic molecules at a magnetic field $B_0 = 16.4$ T. We recorded the changes in signal enhancement, paramagnet-induced quenching and depolarization effects, DNP build-up rate, and Boltzmann polarization. For these samples, the increases in MAS-induced depolarization and DNP build-up times at around 30 K were not as severe as anticipated. As such, we determined that MAS DNP at 30 K provided ~10 times higher sensitivity than MAS DNP at 90 K, which corresponds to the acceleration of experiments by multiplicative factors of up to 100.

1. Introduction

Solid-state nuclear magnetic resonance (NMR) spectroscopy is unique in its ability to elucidate the structure and dynamics of non-crystalline solids at atomic resolution, but suffers from intrinsically low sensitivity. The most promising solution to this dilemma is hyperpolarization. Among the developed hyperpolarization techniques, dynamic nuclear polarization (DNP) is unique in its ability to hyperpolarize a vast array of materials without chemical modification, by relying on the transfer of magnetization from unpaired electron spins. Recent advances in high-field DNP, including the development of high-power, high-frequency, microwave sources (gyrotrons),^{1, 2} low-temperature magic angle spinning (MAS) probes,^{3, 4} and biradical polarizing agents for cross-effect DNP,^{5, 6} have revolutionized solid-state NMR, yielding 2-3 orders of magnitude gains in sensitivity over conventional MAS NMR at moderate external magnetic field strengths B_0 of 9.4 and 14.1 T.

MAS DNP is increasingly utilized in chemistry, structural biology and materials science. The studies of surfaces have particularly

benefitted from DNP, especially those involving low- γ /low-abundance nuclei and/or coverages that are undetectable by conventional MAS NMR.⁷⁻²⁰ This distinguishing performance results from the fact that the polarization source, namely the solutions of biradical species, can be readily introduced at surfaces by incipient wetness impregnation,⁸ and that spectral resolution is largely temperature-independent in such systems.

Despite these successes, MAS DNP has yet to reach its full potential, with nuclear polarizations remaining well below 1%, even with a state-of-the-art instrumentation. It is possible, however, to increase polarization of the electrons, and in doing so nuclear hyperpolarization as well, by increasing B_0 and/or reducing temperature. In conventional NMR, high magnetic fields are preferred given that they additionally increase spectral resolution, particularly for quadrupolar nuclei of importance in materials science.²¹⁻²⁴ DNP efficiency via cross-effect, however, scales roughly linearly with B_0^{-1} and as such generally sees considerable efficiency losses at higher magnetic field.²¹⁻²⁴ These losses can be mitigated by reducing the sample temperature as this both increases the polarization of the source electrons and improves the efficiency of electron-nuclear polarization transfers by lengthening spin relaxation times. Although current DNP instrumentation operates typically at a temperature T of about 100 K utilizing relatively simple and economical nitrogen-based MAS systems,^{3, 4, 25} MAS DNP operated below ~100 K achieved using cold helium (He) gas is starting to draw increased attention due to the said potential for transformative boost in sensitivity.²⁶⁻³⁵ As an added benefit, such low

^a Institute for Protein Research, Osaka University, Suita, Osaka 565-0871, Japan.

^b Center for Quantum Information and Quantum Biology, Institute for Open and Transdisciplinary Research Initiatives, Osaka University.

^c Ames Laboratory, U.S. Department of Energy, Ames, Iowa 50011-3020, United States.

^d Department of Chemistry, Iowa State University, Ames, Iowa 50011-3020, United States.

† Electronic Supplementary Information (ESI) available: See DOI: 10.1039/x0xx00000x

temperature approach offers the possibility of reducing the thermal noise by cooling of the probe end of the RF circuit.³⁶

To enable longer-term operation, an important requirement for multi-dimensional spectroscopy, He must be somehow recycled after it passes through the MAS module. Conventional approaches to He-cooled MAS, however, treat He as an expendable resource, requiring large amounts of expensive liquid He.^{26, 32} By using He to cool and propel the MAS rotors, Barnes et al. achieved ν_R of 8.5 kHz at ~ 6 K; however, they reported very large consumption of liquid He (30 L/h).³⁵ Thurber and Tycko used He to cool and N_2 to spin, achieving an MAS rate ν_R of ~ 7 kHz at 25 K with reduced consumption of liquid He (~ 1.3 L/h).^{32,37} However, the exhausted He was contaminated with N_2 , which challenges the viability of the recycling process. The closed-cycle, completely liquid-He-free, MAS DNP probe system recently reported by some of the present authors represents a milestone toward this end.^{29, 38} In this system, streams of compressed He gas are cooled on the fly using electrical gas chillers before being sent to the NMR probe. The return gas is then immediately recycled, in situ, to sustain long-term (>weeks), highly stable (± 3 Hz), MAS at ~ 30 K without any He loss. A similar system has been reported by De Paëpe et al.,^{30, 33} wherein closed-cycle He gas streams are cooled using a liquid He heat exchanger.

The aforementioned early He-cooled DNP systems offered encouraging results, with enhancements typically increasing when reducing the temperature and build-up times remaining relatively constant. Specifically, Thurber et al. reported a 4.3-fold increase in enhancement from 6 at 80 K to 26 at 16 K for a static alanine solution doped with 20 mM TOTAPOL using a low power solid-state microwave source and a magnetic field of 9.4 T.³⁹ Here, the DNP enhancement is defined as the ratio of the signal intensities obtained with (I_{on}) and without (I_{off}) microwave irradiation at temperature T, $\epsilon_{on/off,T} = I_{on,T}/I_{off,T}$. Note that the $\epsilon_{on/off}$ values do not account for changes in Boltzmann polarization. Under MAS conditions, ($\nu_R \sim 6.7$ kHz), $\epsilon_{on/off}$ was observed to increase ~ 10 -fold from $\epsilon_{on/off,88} = 13$ to $\epsilon_{on/off,25} = 128$ using a triradical polarizing agent and a low power microwave tube (EIO).³² In a similar comparison, Matsuki et al. reported a 2.1-fold increase of DNP enhancement factor from $\epsilon_{on/off,90} = 11$ to $\epsilon_{on/off,35} = 23$ using a high-power gyrotron as the microwave source for a homogeneous urea solution doped with 20 mM TOTAPOL under static conditions at $B_0 = 14.1$ T.²⁶ Using the same apparatus and sample, they observed a 1.3-fold increase from $\epsilon_{on/off,60} = 36$ to $\epsilon_{on/off,47} = 45$ under MAS conditions ($\nu_R \sim 3$ kHz).²⁶

A 2014 paper by Thurber and Tycko, however, added an important caveat to these earlier results by noting that a process known as nuclear depolarization, caused by a reverse cross-effect mechanism in the absence of microwaves, was partly responsible for the increases in $\epsilon_{on/off}$ observed at ~ 25 K.⁴⁰ Briefly, due to increases in the electron spin-lattice relaxation rate, T_{1e} , depolarization is more efficient at lower temperatures, decreasing I_{off} and artificially inflating $\epsilon_{on/off}$. De Paëpe et al. later corroborated these results, measuring a ~ 3 -fold increase in $\epsilon_{on/off}$ at 36 K under ~ 10 kHz MAS, but noted proportional decrease in I_{off} due to the depolarization effect.³⁰ Among the few reported applications of He-cooled MAS DNP is the study of the surface of γ -alumina via ^{27}Al nuclei at 9.4 T; however, neither $\epsilon_{on/off}$ nor depolarization effects were measured directly on ^{27}Al .³⁰ Most recently, Barnes et al reported enhancement

of ^{13}C signals from human cells at 7 T, in which $\epsilon_{on/off}$ decreased from $\epsilon_{on/off,90} = 57$ to $\epsilon_{on/off,6} = 46$ under MAS (~ 6 kHz).³⁴

With the earlier assessments of the scale and mechanisms of sensitivity improvements at low temperatures being focused on dissolved molecules or solvents, we turn here to a case study involving a surface-bound species at 16.4 T. Considering the potential impact that He-cooled MAS DNP may have on materials science and heterogeneous catalysis, where the characterization of surfaces and interfaces is an everlasting challenge, we opted to study an organically surface-modified mesoporous silica nanoparticle (MSN) sample. In addition, a homogeneous urea frozen solution was studied as a benchmark sample. The effects of low temperatures (~ 30 to 100 K) on the signal enhancement, paramagnet-induced quenching, depolarization effects, DNP build-up rates, and Boltzmann changes are all considered here.

2. Experiments

2.1. Sample Preparations.

3-(*N*-phenylureido)propyl-functionalized mesoporous silica nanoparticles (PUP-MSN) were synthesized using a previously reported method.⁴¹ The dry PUP-MSN powder was mixed with deionized water doped with 10 mM AMUPol. Our earlier study identified the solution of AMUPol in regular water or TEKPol in 1,1,2,2-tetrachloroethane as the best sample formulations for DNP measurements on PUP-MSN at 9.4 T and 100 K.⁴² The performance of TEKPol, however, decreases significantly at higher magnetic field,⁴³ and indeed we observed a very low enhancement of 1–3 at 90 K for the samples studied here (spectra are not shown). A total of 26 mg was center-packed in 3.2-mm Si_3N_4 rotors using Kel-F spacers, corresponding to ~ 24 μ mol of the natural abundance PUP moiety. ^{13}C -labeled urea (2 M) was dissolved in a standard DNP matrix (d_8 -glycerol/ $D_2O/H_2O = 6.5/2.5/1$ w/w/w) together with 10 mM AMUPol⁴⁴ as the polarizing agent.

One of the spacers was hollowed out and packed with a small amount of KBr powder, which was used as an internal thermometer.⁴⁵ The Vespel® turbine and bottom caps were specially designed to tighten at He-cooled conditions and loosen at room temperature, facilitating repeated use.⁴⁶

2.2. DNP MAS NMR.

All He-cooled MAS DNP experiments were performed at $B_0 = 16.4$ T on a 700 MHz solid-state NMR spectrometer (ECA-700II, JEOL RESONANCE Inc.) equipped with a home-built continuous-wave 460 GHz gyrotron⁴⁷ and a closed-cycle He-cooling MAS probe system.²⁹ The MAS rates achievable with this probe are 8 kHz at 20 K, 12 kHz at 30 K, 14 kHz at 60 K, and 18 kHz at 90 K. The 1H and ^{13}C Larmor frequencies were 698.66 MHz and 175.67 MHz, respectively. The gyrotron uses a 10 T cryogen-free superconducting magnet (JM-TD-10T100, JASTEC), and oscillates at the second harmonic mode producing high-power (~ 8 W) microwaves at 460 GHz. While the microwave frequency is tunable over a range of ~ 0.6 GHz, all measurements presented in this work were performed at a fixed frequency of 459.95 GHz, which maximized the enhancements with AMUPol. The frequency-dependence of DNP enhancement factor measured for the urea sample can be found in the Electronic

Supplementary Information (ESI,† Fig. S1). Also shown in Fig. S2 in ESI† is the plot representing the signal enhancements as a function of microwave power measured for the urea sample at three different temperatures. Importantly, the ratios of the signal enhancements measured at any given temperature remain independent of power within the measurement error.

All the $^{13}\text{C}\{^1\text{H}\}$ cross-polarization (CP) MAS spectra were collected under ~ 6 kHz MAS and the sample temperature was changed between ~ 90 K and ~ 30 K. The reported temperatures were measured within the rotor using the ^{79}Br T_1 relaxation time of KBr.⁴⁵ The ^1H radiofrequency (RF) amplitudes were set to 75, 30, and 70 kHz for the excitation pulse, contact pulse, and heteronuclear ^1H decoupling, respectively. The ^{13}C RF field amplitude used during CP was set to ~ 20 kHz. The spectra were recorded by averaging 2 to 128 transients, and the spectral intensity was normalized to the number of transients to yield the intensity “per scan”. All the reported chemical shifts are relative to sodium 2,2-dimethyl-2-silapentane-5-sulfonate (DSS). The recycle delay, τ_{rd} , for all measurements was set to $1.3\tau_{\text{DNP}}$, where τ_{DNP} is the time constant obtained when fitting a saturation recovery experiment under microwave irradiation with the expression: $1 - \exp(\tau/\tau_{\text{DNP}})$, where τ is the recovery time.

3. Results and Discussion

3.1. Enhancement factors.

Fig. 1 shows $^{13}\text{C}\{^1\text{H}\}$ CPMAS spectra of PUP-MSN and urea recorded at several temperatures between 30 and 90 K, with and without microwave irradiation. In the PUP-MSN spectra (Fig. 1a), the signals from the C1, C2, and C3 carbons are clearly resolved (at 10, 24, and 42 ppm, respectively), while the signals of aromatic and carbonyl carbons C4–C8 are only partially resolved due to overlap with each other’s spinning sidebands. A sideband-free spectrum of PUP-MSN can be found in our earlier study.⁴¹ The spectra of urea (Fig. 1b) exhibit a single peak at ~ 160 ppm flanked by spinning sidebands. The signals from deuterated glycerol (at ~ 63 and ~ 72 ppm) are only barely visible in the microwave-on spectra. The spectral intensities discussed below were evaluated by integrating the entire spectral area for PUP-MSN, or the centerband and two flanking (± 1) spinning sidebands for urea. Thus, the effects of the spectral overlap and the small glycerol signal are safely ignored in the discussion.

As has been previously emphasized, a rigorous assessment of the sensitivity gain from DNP must include multiple contributions,^{22, 41, 48, 49} which we briefly describe below.

- (1) The DNP enhancement factor $\varepsilon_{\text{on/off},T}$ was defined above as the ratio of integrated spectral intensities obtained per scan with and without microwave irradiation at temperature T (K). Since our focus is on the effect of lowering the sample temperature from around 90 K down, we also define the relative change of

$$\varepsilon_{\text{on/off}} \text{ as } [\varepsilon_{\text{on/off}}] \equiv \frac{\varepsilon_{\text{on/off},T}}{\varepsilon_{\text{on/off},90}}.$$

- (2) It is well recognized that the $\varepsilon_{\text{on/off},T}$ factor overestimates the sensitivity gain from DNP because it does not include the effects

of the paramagnetic quenching $\varepsilon_{\text{quench}}$ and the MAS-induced depolarization $\varepsilon_{\text{depo}}$.^{24, 40, 50-54} The former is due to unobservability of nuclei that are within a few Angstroms of unpaired electrons,^{50, 51} while the latter leads to a reduction in polarization due to a reverse cross-effect mechanism in the absence of microwave irradiation.^{40, 52, 53} The overall paramagnet-induced signal change per scan ε_{θ} , is given by $\varepsilon_{\theta} = \varepsilon_{\text{quench}} \times \varepsilon_{\text{depo}}$, and is often referred to as the contribution factor (note that higher values of ε_{θ} correspond to lower losses).^{40, 53} After correcting for ε_{θ} , which is known to be temperature-dependent, the net DNP enhancements, denoted as $\varepsilon_{\text{net},T}$ and $[\varepsilon_{\text{net},T}]$, are given by $\varepsilon_{\text{net},T} = \varepsilon_{\text{on/off},T} \varepsilon_{\theta,T}$ and $[\varepsilon_{\text{net},T}] = \frac{\varepsilon_{\text{net},T}}{\varepsilon_{\text{net},90}}$. We note that in principle $\varepsilon_{\text{depo},T}$, $\varepsilon_{\text{quench}}$ and ε_{θ} can be determined experimentally from the following measurements performed in the absence of microwaves: $\varepsilon_{\text{depo}}$ as a ratio of signal intensities observed under MAS versus static conditions in a sample containing radicals, ε_{θ} as a ratio of signals obtained under MAS from doped and undoped samples, and $\varepsilon_{\text{quench}}$ as a ratio of signals from doped and undoped samples under the static condition. In principle, it is easiest to measure ε_{θ} and $\varepsilon_{\text{depo}}$, and determine $\varepsilon_{\text{quench}}$ as the ratio between the two.

- (3) The sensitivity analysis must also account for the effect of temperature on the rate of the polarization build-up and its effect on the number of scans acquired in a given unit of time.⁵⁵

This contribution introduces an additional factor of $\sqrt{\frac{\tau_{\text{DNP},90}}{\tau_{\text{DNP},T}}}$, where $\tau_{\text{DNP},T}$ and $\tau_{\text{DNP},90}$ denote the DNP build-up times at temperatures T and 90 K, respectively.

- (4) Lastly, both nuclear and electron polarizations are defined by Boltzmann distribution, and thus grow considerably at very low temperatures. Although for all nuclei, the so-called high temperature approximation and the resulting Curie law are still completely valid in the temperature range used in this study, for the electrons there is about 10% deviation at $T = 30$ K. Nevertheless, we will ignore this small divergence and use a simple additional factor T_0/T , where in our study $T_0 = 90$ K. In such case, the overall sensitivity gain resulting from lowering the temperature from 90 K to T is given by

$$[\varepsilon_{\text{time},T}] = [\varepsilon_{\text{net},T} \varepsilon_{\text{other}}] \times \frac{90\text{K}}{T} \times \sqrt{\frac{\tau_{\text{DNP},90}}{\tau_{\text{DNP},T}}}. \quad (1)$$

We included in eqn (1) is an additional factor, $\varepsilon_{\text{other}}$, to account for the effect of cooling on CP efficiency, NMR linewidth, thermal noise and RF efficiency (i.e., probe quality factor), which may all influence the sensitivity of the experiment, but strongly depend on the sample setup, instrument, and experiment design.⁴¹ The significance of the last two contributions will be assessed by measuring the temperature dependence of the signal intensity in undoped samples. Experimentally, $[\varepsilon_{\text{time},T}]$ is determined as:

$$[\varepsilon_{\text{time},T}]_{\text{exp}} = \frac{I_{\text{on},T}}{I_{\text{on},90\text{K}}} \times \sqrt{\frac{\tau_{\text{DNP},90}}{\tau_{\text{DNP},T}}}. \quad (2)$$

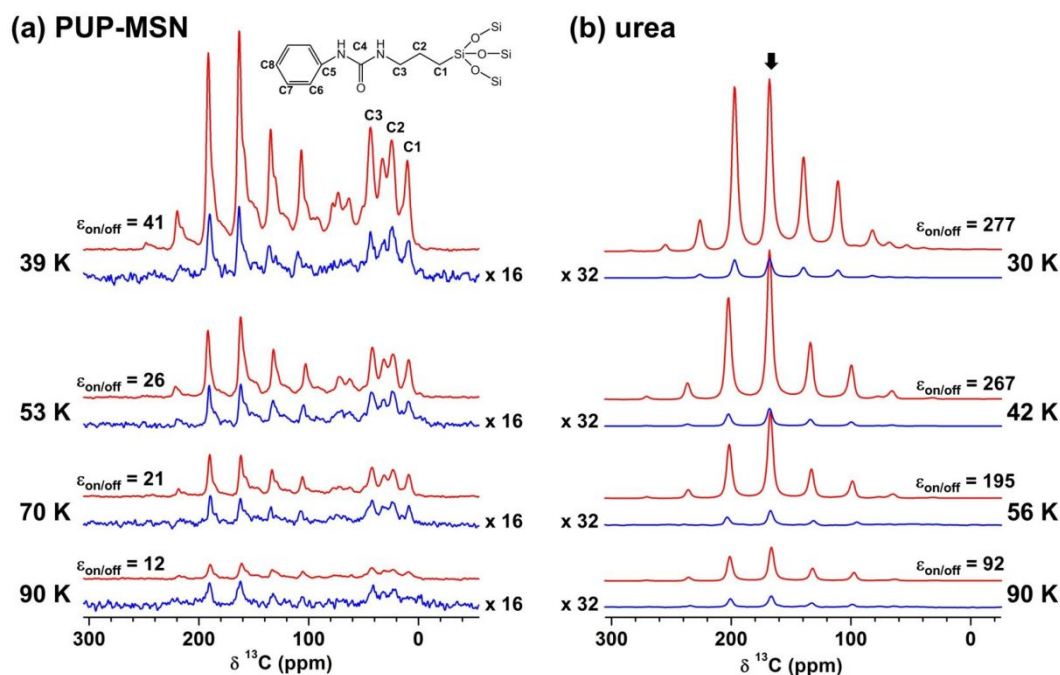


Fig. 1 DNP-enhanced $^{13}\text{C}\{^1\text{H}\}$ CPMAS spectra of PUP-MSN (a) and urea (b) obtained at indicated sample temperatures and $\nu_R = 6$ kHz. Red and blue lines represent the spectra taken with and without microwave irradiation, respectively. In (a), the resolved peaks are labelled in accordance with the molecular structure shown. In (b) the arrow marks the centerband.

In Fig. 2 the enhancement factors $\epsilon_{\text{on/off},T}$, $\epsilon_{\text{net},T}$, $[\epsilon_{\text{on/off},T}]$ and $[\epsilon_{\text{net},T}]$ are plotted as function of temperature for both samples, PUP-MSN and urea. A monotonic increase in $\epsilon_{\text{on/off}}$ was observed with reduction of sample temperatures from ~ 90 K down to $\sim 39/30$ K (ESI,† see also Table S1). Note that the enhancement factors $\epsilon_{\text{on/off}}$ for PUP-MSN were 7-10 times smaller than those obtained for urea over the entire

temperature range. However, the relative gain in enhancement from lowering the temperature was higher for PUP-MSN ($[\epsilon_{\text{on/off},39}] = 3.4$) than for urea ($[\epsilon_{\text{on/off},30}] = 3.0$). The origin of these observations is in the temperature dependence of $\epsilon_{\theta,T}$, as we discuss below.

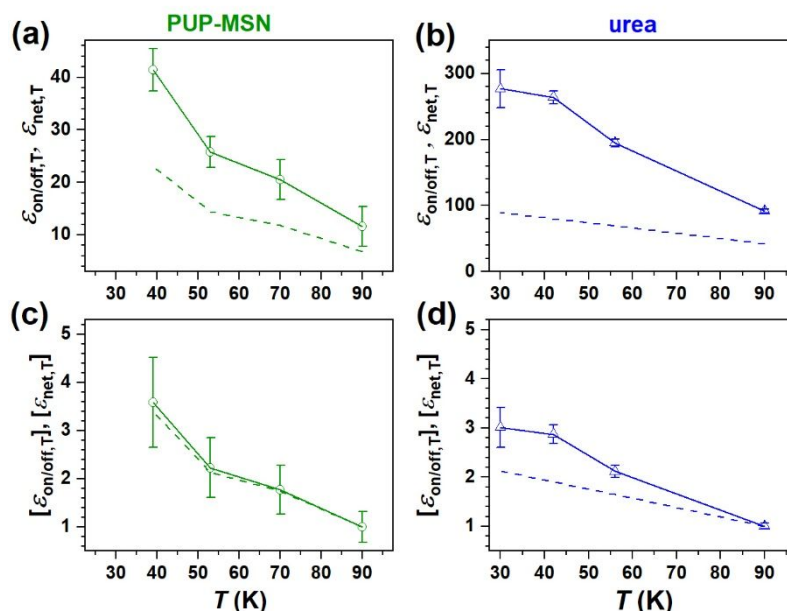


Fig. 2 Temperature dependence of $\epsilon_{\text{on/off},T}$ and $\epsilon_{\text{net},T}$ (a, b) and $[\epsilon_{\text{on/off},T}]$ and $[\epsilon_{\text{net},T}]$ (c, d). Dashed lines show the DNP enhancement corrected for $\epsilon_{\theta,T}$, i.e. $\epsilon_{\text{net},T} = \epsilon_{\text{on/off},T} \times \epsilon_{\theta,T}$ (a, b) and $[\epsilon_{\text{net},T}]$ (c, d). The data are shown for PUP-MSN (a, c) and urea (b, d) samples. The errors were estimated from the signal-to-noise ratio of the microwave-off spectra.

ARTICLE

3.2. Signal bleaching and depolarization.

The temperature dependence of the contribution factor $\epsilon_{\theta,T}$ measured for PUP-MSN and urea is plotted in Fig. 3a. A gradual decrease of $\epsilon_{\theta,T}$ with lowering of sample temperatures from ~ 90 K to ~ 30 K was observed for both samples: the effect was fairly minor for PUP-MSN (5% change from 0.59 to 0.56) while that for urea was more considerable (30% change from 0.46 to 0.32). Since ϵ_{quench} is not sensitive to temperature (as verified for the urea sample where $\epsilon_{\text{quench}} = 0.83$ at both 90 and 30 K), the decrease of $\epsilon_{\theta,T}$ was attributed solely to nuclear depolarization $\epsilon_{\text{depo},T}$.^{40, 52, 53} Overall, these paramagnetic losses were not as severe for the samples used in the present study in contrast to the experiments reported earlier at 9.4 T, where a three-fold increase of depolarization was observed for a γ -alumina sample containing AMUPol upon lowering the temperature from 105 K to 36 K.³⁰ After correcting for $\epsilon_{\theta,T}$, the net DNP enhancement amounted to $\epsilon_{\text{net},39} = 23$ for PUP-MSN and $\epsilon_{\text{net},30} = 89$ for urea, corresponding to the net DNP gains relative to 90 K-DNP, $[\epsilon_{\text{net},90}]$ of 3.2 and 2.0, respectively (Fig. 2c and d). The facts that the $[\epsilon_{\text{net},T}]$ values for both samples were significantly greater than unity and that they monotonically increased with decreases in temperature indicate that the gains in DNP performance generally outweigh the increase in MAS-induced depolarization at lower temperatures. Especially, a large increase in the DNP performance was observed between 50 K and 39 K for PUP-MSN (Fig. 2c). It is also remarkable that, similarly to the $[\epsilon_{\text{on/off},T}]$ values, the value of $[\epsilon_{\text{net},T}]$ observed for PUP-MSN was higher than that for the urea sample; in other words, PUP-MSN exhibits a larger sensitivity benefit from DNP at a temperature below ~ 100 K. This is partly due to the relatively temperature-independent $\epsilon_{\theta,T}$ of the PUP-MSN sample but also due to differences in nuclear relaxation as discussed below.

It is interesting to speculate upon why PUP-MSN exhibited a much higher (and relatively temperature-independent) $\epsilon_{\theta,T}$ and lower $\epsilon_{\text{on/off},T}$ values than the urea sample over the entire temperature range. Given that there are no reactive chemical groups on the MSN surface that may chemically reduce radicals,⁵⁶ the high $\epsilon_{\theta,T}$ and low $\epsilon_{\text{on/off},T}$ are not likely to have originated from a depleted polarization source. Keeping in mind that we used the same polarizing agent (AMUPol) in all of our experiments, this result is most likely due to the shorter ^1H relaxation time and the larger pool of polarizable nuclei within the PUP-MSN sample.⁵⁷⁻⁵⁹ Indeed, a simple estimate showed that the ratio of the number of ^1H s to that of electron spins in the PUP-MSN sample was at least twice that of the urea samples, while the intrinsic $T_{1\text{H}}$ measured for undoped samples was nearly an order of magnitude longer for urea (58 s) than for PUP-MSN (9 s) at ~ 90 K.

Additional insight may be gained from the analysis of relative contributions to $\epsilon_{\theta,T}$ from $\epsilon_{\text{depo},T}$ and ϵ_{quench} . For the urea sample, we observed experimentally that MAS-induced depolarization is less detrimental at higher magnetic field (specifically, $\epsilon_{\text{depo},90} = 0.56$ at

16.4 T and $\epsilon_{\text{depo},100} = 0.41$ at 9.4 T), while paramagnetic quenching, given by the ratio $\epsilon_{\theta,T}/\epsilon_{\text{depo},T}$, remains constant ($\epsilon_{\text{quench}} = 0.83$ at 16.4 T, and $\epsilon_{\text{quench},100} = 0.82$ at 9.4 T). For PUP-MSN, the estimates are quite different: at 9.4 T we obtained $\epsilon_{\text{depo},100} = 0.94$ and $\epsilon_{\text{quench},100} = 0.63$ (ESI,[†] see Fig. S3), whereas at 16.4 T the $\epsilon_{\text{depo},90}$ value of 0.92 was derived assuming the field-independent quenching factor of 0.63. These estimations suggest that the higher $\epsilon_{\theta,T}$ for PUP-MSN is attributed to the higher $\epsilon_{\text{depo},T}$ (i.e. less depolarization). The relative lack of depolarization in PUP-MSN is consistent with the limited diffusion of polarization in the sample, which inhibits (de)polarization of the nuclei situated away from the radical. This analysis is also supported by the biexponential nature of the DNP build-up curves for the PUP-MSN sample (ESI,[†] Fig. S4).

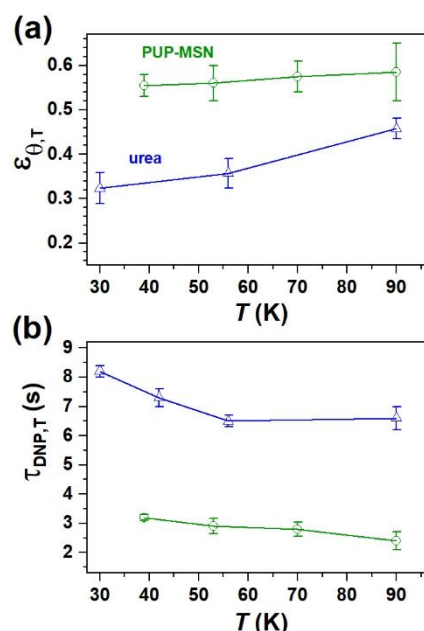


Fig. 3 Temperature dependence of $\epsilon_{\theta,T}$ (a) and $\tau_{\text{DNP},T}$ (b) measured for PUP-MSN and urea.

3.3. DNP build-up time.

Fig. 3b plots the temperature dependence of the polarization build-up time constant, $\tau_{\text{DNP},T}$, measured with a saturation recovery experiment under microwave irradiation. In general, slower build-up is expected at lower sample temperatures, which is a potential drawback of DNP operated below ~ 100 K. Only a small increase of τ_{DNP} , however, was observed with the temperature drop for PUP-MSN (from $\tau_{\text{DNP},90} = 2.4$ s to $\tau_{\text{DNP},39} = 3.2$ s) and urea (from $\tau_{\text{DNP},90} = 6.6$ s to $\tau_{\text{DNP},30} = 8.2$ s). The resulting negative effect on unit-time sensitivity, $[\epsilon_{\text{time},T}]$, was insignificant (0 – 12%). It thus appears that the build-up time is determined by the rate at which the radical can hyperpolarize, and the size of the proton bath, which are both largely temperature-independent properties within this temperature range.

The observed $\tau_{\text{DNP},T}$ were in general considerably shorter than the intrinsic $T_{1H,T}$ due to cross-effect and paramagnetic relaxation enhancement (PRE) from the polarizing agent.⁵⁹

3.4. Curie factor and overall unit-time sensitivity.

Fig. 4 plots the temperature dependence of the overall sensitivity gains given by eqn (2). The overall measured sensitivity gain was a factor of 11.1 and 7.3 higher than that with the DNP at ~ 90 K for PUP-MSN and urea, respectively, corresponding to 123 and 53-fold acquisition time savings. These results clearly illustrate a definitive improvement of the cross-effect DNP efficiency by lowering the sample temperature below ~ 100 K for both surface-supported species and homogeneous solution.

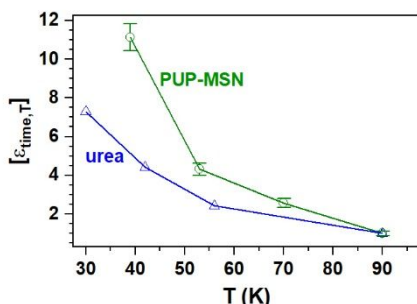


Fig. 4 Overall sensitivity enhancements relative to DNP at 90 K estimated by eqn (2) as a function of temperature.

Upon lowering the temperature from ~ 90 K to ~ 30 K, the increases in I_{off} for undoped samples were 10 – 30 % higher than those expected from Boltzmann increases alone (ESI,† Fig. S5). The increase in I_{off} is mainly attributable to the improved coil efficiency, which thus represents an additional sensitivity enhancement when performing MAS DNP experiments below ~ 100 K. We also note that for the present setup a reduction in thermal noise was not observed. Simply cooling the RF coil and tuning/matching capacitors in the probe alone does not significantly reduce thermal noise; cryogenic-cooling of the preamplifier, as realized with a cryogenic duplexer, is required to fully benefit from noise reduction.^{36,60}

4. Conclusions

We have assessed, at $B_0 = 16.4$ T, the sensitivity benefit from performing MAS DNP NMR measurements at around 30 K, using a state-of-the-art closed-cycle He-based MAS DNP probe system. Various contributions affecting the sensitivity gain were studied in two types of samples: surface-functionalized mesoporous silica nanoparticles (PUP-MSN) doped with 10 mM AMUPol in water, and a homogeneous solution of ^{13}C -urea in a DNP matrix with 10 mM AMUPol. The microwave-on/off enhancement factors, $\epsilon_{\text{on/off}}$, for these two samples were 41 (39 K) and 277 (30 K), respectively. Decrease in the contribution factor and increase in the DNP build-up time observed at lower temperatures were not as severe as previously anticipated. Consequently, the sensitivity at around 30 K exceeded that with DNP at 90 K by additional factors of 11.1 and 7.3 for the two samples, corresponding to 123 and 53-fold time savings. PUP-MSN showed a larger improvement in the DNP enhancement than urea sample with lowering temperature. We suspect that MAS DNP operated at sample temperatures much lower than 100 K is able

to significantly restrict PUP chain motions and lengthen its intrinsically shorter T_{1H} , which increases the fraction of the PUP groups that are efficiently hyperpolarized. Along these lines, we expect that systems involving methyl groups, a common source of relaxation,⁶¹ may benefit the most from low-temperature DNP.⁶²

Conflicts of interest

There are no conflicts to declare.

Acknowledgements

This work was supported by JST SENTAN (H271030 and JPMJSN15A1), the Ministry of Education, Culture, Sports, Science and Technology (MEXT), Japan (480790) (Y.M., T.F.), the U.S. Department of Energy, Office of Basic Energy Sciences, Division of Chemical Sciences, Geosciences, and Biosciences, and by the laboratory-directed research and development (LDRD) program at the Ames Laboratory (T.K., F.A.P). The Ames Laboratory is operated for the U.S. Department of Energy by Iowa State University under Contract No. DE-AC02-07CH11358. We thank Prof. I. I. Slowing for kindly providing the sample of PUP-MSN used in this study.

References

- 1 S. Sabchevski, T. Idehara, S. Mitsudo and T. Fujiwara, *Int. J. Infrared Millimeter Waves*, 2005, **26**, 1241-1264.
- 2 C. D. Joye, R. G. Griffin, M. K. Hornstein, K. N. Hu, K. E. Kreischer, M. Rosay, M. A. Shapiro, J. R. Sirigiri, R. J. Temkin and P. P. Woskov, *IEEE Transactions on Plasma Science*, 2006, **34**, 518-523.
- 3 M. Rosay, J. C. Lansing, K. C. Haddad, W. W. Bachovchin, J. Herzfeld, R. J. Temkin and R. G. Griffin, *J. Am. Chem. Soc.*, 2003, **125**, 13626-13627.
- 4 A. B. Barnes, M. L. Mak-Jurkauskas, Y. Matsuki, V. S. Bajaj, P. C. A. van der Wel, R. DeRocher, J. Bryant, J. R. Sirigiri, R. J. Temkin, J. Lugtenburg, J. Herzfeld and R. G. Griffin, *J. Magn. Reson.*, 2009, **198**, 261-270.
- 5 K. N. Hu, H. H. Yu, T. M. Swager and R. G. Griffin, *J. Am. Chem. Soc.*, 2004, **126**, 10844-10845.
- 6 C. S. Song, K. N. Hu, C. G. Joo, T. M. Swager and R. G. Griffin, *J. Am. Chem. Soc.*, 2006, **128**, 11385-11390.
- 7 O. Lafon, M. Rosay, F. Aussenac, X. Y. Lu, J. Trebosc, O. Cristini, C. Kinowski, N. Touati, H. Vezin and J. P. Amoureux, *Angew. Chem. Int. Ed.*, 2011, **50**, 8367-8370.
- 8 A. Lesage, M. Lelli, D. Gajan, M. A. Caporini, V. Vitzthum, P. Miéville, J. Alauzun, A. Roussey, C. Thieuleux, A. Mehdi, G. Bodenhausen, C. Copéret and L. Emsley, *J. Am. Chem. Soc.*, 2010, **132**, 15459-15461.
- 9 A. Zagdoun, G. Casano, O. Ouari, G. Lapadula, A. J. Rossini, M. Lelli, M. Baffert, D. Gajan, L. Veyre, W. E. Maas, M. Rosay, R. T. Weber, C. Thieuleux, C. Copéret, A. Lesage, P. Tordo and L. Emsley, *J. Am. Chem. Soc.*, 2012, **134**, 2284-2291.
- 10 A. J. Rossini, A. Zagdoun, M. Lelli, J. Canivet, S. Aguado, O. Ouari, P. Tordo, M. Rosay, W. E. Maas, C. Coperet, D.

- Farrusseng, L. Emsley and A. Lesage, *Angew. Chem. Int. Ed.*, 2012, **51**, 123-127.
- 11 F. Blanc, L. Sperrin, D. A. Jefferson, S. Pawsey, M. Rosay and C. P. Grey, *J. Am. Chem. Soc.*, 2013, **135**, 2975-2978.
- 12 Z. Guo, T. Kobayashi, L.-L. Wang, T. W. Goh, C. Xiao, M. A. Caporini, M. Rosay, D. D. Johnson, M. Pruski and W. Huang, *Chem. Euro. J.*, 2014, **20**, 16308-16313.
- 13 N. Eedugurala, Z. Wang, U. Chaudhary, N. Nelson, K. Kandel, T. Kobayashi, I. I. Slowing, M. Pruski and A. D. Sadow, *ACS Catal.*, 2015, **5**, 7399-7414.
- 14 F. A. Perras, T. Kobayashi and M. Pruski, *J. Am. Chem. Soc.*, 2015, **137**, 8336-8339.
- 15 D. Lee, C. Leroy, C. Crevant, L. Bonhomme-Coury, F. Babonneau, D. Laurencin, C. Bonhomme and G. De Paepe, *Nature Commun.*, 2017, **8**, 14104.
- 16 A. J. Rossini, A. Zagdoun, M. Lelli, A. Lesage, C. Coperet and L. Emsley, *Acc. Chem. Res.*, 2013, **46**, 1942-1951.
- 17 T. Kobayashi, F. A. Perras, Slowing, II, A. D. Sadow and M. Pruski, *ACS Catal.*, 2015, **5**, 7055-7062.
- 18 A. S. L. Thankamony, J. J. Wittmann, M. Kaushik and B. Corzilius, *Prog. Nucl. Magn. Reson. Spectrosc.*, 2017, **102**, 120-195.
- 19 F. A. Perras, T. Kobayashi and M. Pruski, *eMagRes*, 2018, **7**, 35-50.
- 20 W. C. Liao, B. Ghaffari, C. P. Gordon, J. Xu and C. Coperet, *Current Opinion in Colloid & Interface Science*, 2018, **33**, 63-71.
- 21 N. J. Brownbill, D. Gajan, A. Lesage, L. Emsley and F. Blanc, *Chem. Commun.*, 2017, **53**, 2563-2566.
- 22 S. R. Chaudhari, D. Wisser, A. C. Pinon, P. Berruyer, D. Gajan, P. Tordo, O. Ouari, C. Reiter, F. Engelke, C. Coperet, M. Lelli, A. Lesage and L. Emsley, *J. Am. Chem. Soc.*, 2017, **139**, 10609-10612.
- 23 F. Mentink-Vigier, I. Marin-Montesinos, A. P. Jagtap, T. Halbritter, J. van Tol, S. Hediger, D. Lee, S. T. Sigurdsson and G. De Paepe, *J. Am. Chem. Soc.*, 2018, **140**, 11013-11019.
- 24 D. Wisser, G. Karthikeyan, A. Lund, G. Casano, H. Karoui, M. Yulikov, G. Menzildjian, A. C. Pinon, A. Porea, F. Engelke, S. R. Chaudhari, D. Kubicki, A. J. Rossini, I. B. Moroz, D. Gajan, C. Coperet, G. Jeschke, M. Lelli, L. Emsley, A. Lesage and O. Ouari, *J. Am. Chem. Soc.*, 2018, **140**, 13340-13349.
- 25 B. J. Albert, S. H. Pahng, N. Alaniva, E. L. Sesti, P. W. Rand, E. P. Saliba, F. J. Scott, E. J. Choi and A. B. Barnes, *J. Magn. Reson.*, 2017, **283**, 71-78.
- 26 Y. Matsuki, K. Ueda, T. Idehara, R. Ikeda, I. Ogawa, S. Nakamura, M. Toda, T. Anai and T. Fujiwara, *J. Magn. Reson.*, 2012, **225**, 1-9.
- 27 A. Potapov, K. R. Thurber, W. M. Yau and R. Tycko, *J. Magn. Reson.*, 2012, **221**, 32-40.
- 28 K. R. Thurber, A. Potapov, W. M. Yau and R. Tycko, *J. Magn. Reson.*, 2013, **226**, 100-106.
- 29 Y. Matsuki, S. Nakamura, S. Fukui, H. Suematsu and T. Fujiwara, *J. Magn. Reson.*, 2015, **259**, 76-81.
- 30 E. Bouleau, P. Saint-Bonnet, F. Mentink-Vigier, H. Takahashi, J. F. Jacquot, M. Bardet, F. Aussenac, A. Porea, F. Engelke, S. Hediger, D. Lee and G. De Paepe, *Chem. Sci.*, 2015, **6**, 6806-6812.
- 31 Y. Matsuki, T. Idehara, J. Fukazawa and T. Fujiwara, *J. Magn. Reson.*, 2016, **264**, 107-115.
- 32 K. Thurber and R. Tycko, *J. Magn. Reson.*, 2016, **264**, 99-106.
- 33 D. Lee, E. Bouleau, P. Saint-Bonnet, S. Hediger and G. De Paepe, *J. Magn. Reson.*, 2016, **264**, 116-124.
- 34 B. J. Albert, C. K. Gao, E. L. Sesti, E. P. Saliba, N. Alaniva, F. J. Scott, S. T. Sigurdsson and A. B. Barnes, *Biochemistry*, 2018, **57**, 4741-4746.
- 35 E. L. Sesti, N. Alaniva, P. W. Rand, E. J. Choi, B. J. Albert, E. P. Saliba, F. J. Scott and A. B. Barnes, *J. Magn. Reson.*, 2018, **286**, 1-9.
- 36 A. Hassan, C. M. Quinn, J. Struppe, I. V. Sergeev, C. T. Zhang, C. M. Guo, B. Runge, T. Theint, H. H. Dao, C. P. Jaroniec, M. Berbon, A. Lends, B. Habenstein, A. Loquet, R. Kuemmerle, B. Perrone, A. M. Gronenborn and T. Polenova, *J. Magn. Reson.*, 2020, **311**, 106680.
- 37 K. R. Thurber and R. Tycko, *J. Magn. Reson.*, 2008, **195**, 179-186.
- 38 Y. Matsuki and T. Fujiwara, in *Handbook of High-Field Dynamic Nuclear Polarization* eds. V. K. Michaelis, R. G. Griffin, B. Corzilius and S. Vega, John Wiley & Sons, 2020.
- 39 K. R. Thurber, W.-M. Yau and R. Tycko, *J. Magn. Reson.*, 2010, **204**, 303-313.
- 40 K. R. Thurber and R. Tycko, *J. Chem. Phys.*, 2014, **140**, 184201.
- 41 T. Kobayashi, O. Lafon, A. S. L. Thankamony, Slowing, II, K. Kandel, D. Carnevale, V. Vitzthum, H. Vezin, J. P. Amoureux, G. Bodenhausen and M. Pruski, *Phys. Chem. Chem. Phys.*, 2013, **15**, 5553-5562.
- 42 T. Kobayashi, F. A. Perras, U. Chaudhary, Slowing, II, W. Y. Huang, A. D. Sadow and M. Pruski, *Solid State Nucl. Magn. Reson.*, 2017, **87**, 38-44.
- 43 M. Valla, A. J. Rossini, M. Caillot, C. Chizallet, P. Raybaud, M. Digne, A. Chaumonnot, A. Lesage, L. Emsley, J. A. van Bokhoven and C. Coperet, *J. Am. Chem. Soc.*, 2015, **137**, 10710-10719.
- 44 C. Sauvée, M. Rosay, G. Casano, F. Aussenac, R. T. Weber, O. Ouari and P. Tordo, *Angew. Chem. Int. Ed.*, 2013, **52**, 10858-10861.
- 45 K. R. Thurber and R. Tycko, *J. Magn. Reson.*, 2009, **196**, 84-87.
- 46 DE102016000863-A1; US2016223628-A1; JP2016142537-A; JP6471518-B2; US10254357-B2.
- 47 T. Idehara, Y. Tatematsu, Y. Yamaguchi, E. M. Khutoryan, A. N. Kuleshov, K. Ueda, Y. Matsuki and T. Fujiwara, *J. Infrared Millimeter Terahertz Waves*, 2015, **36**, 613-627.
- 48 H. Takahashi, D. Lee, L. Dubois, M. Bardet, S. Hediger and G. De Paepe, *Angew. Chem. Int. Ed.*, 2012, **51**, 11766-11769.
- 49 D. Lee, S. Hediger and G. De Paepe, *Solid State Nucl. Magn. Reson.*, 2015, **66-67**, 6-20.
- 50 S. Lange, A. H. Linden, U. Akbey, W. T. Franks, N. M. Loening, B. J. van Rossum and H. Oschkinat, *J. Magn. Reson.*, 2012, **216**, 209-212.
- 51 B. Corzilius, L. B. Andreas, A. A. Smith, Q. Z. Ni and R. G. Griffin, *J. Magn. Reson.*, 2014, **240**, 113-123.
- 52 A. J. P. Linde, S. Chinthalapalli, D. Carnevale and G. Bodenhausen, *Phys. Chem. Chem. Phys.*, 2015, **17**, 6415-6422.

ARTICLE

Journal Name

- 53 F. Mentink-Vigier, S. Paul, D. Lee, A. Feintuch, S. Hediger, S. Vega and G. De Paepe, *Phys. Chem. Chem. Phys.*, 2015, **17**, 21824-21836.
- 54 A. J. Rossini, A. Zagdoun, M. Lelli, D. Gajan, F. Rascon, M. Rosay, W. E. Maas, C. Coperet, A. Lesage and L. Emsley, *Chem. Sci.*, 2012, **3**, 108-115.
- 55 A. Lund, A. Equbal and S. Han, *Phys. Chem. Chem. Phys.*, 2018, **20**, 23976-23987.
- 56 E. Pump, A. Bendjeriou-Sedjerari, J. Viger-Gravel, D. Gajan, B. Scotto, M. K. Samantaray, E. Abou-Hamad, A. Gurinov, W. Almaksoud, Z. Cao, A. Lesage, L. Cavallo, L. Emsley and J. M. Basset, *Chem. Sci.*, 2018, **9**, 4866-4872.
- 57 P. C. A. van der Wel, K. N. Hu, J. Lewandowski and R. G. Griffin, *J. Am. Chem. Soc.*, 2006, **128**, 10840-10846.
- 58 O. Lafon, A. S. L. Thankamony, T. Kobayashi, D. Carnevale, V. Vitzthum, Slowing, II, K. Kandel, H. Vezin, J. P. Amoureux, G. Bodenhausen and M. Pruski, *J. Phys. Chem. C*, 2013, **117**, 1375-1382.
- 59 F. Mentink-Vigier, S. Vega and G. De Paëpe, *Phys. Chem. Chem. Phys.*, 2017, **19**, 3506-3522.
- 60 T. Mizuno and K. Takegoshi, *Rev. Sci. Instrum.*, 2009, **80**, 124702.
- 61 Q. Z. Ni, E. Markhasin, T. V. Can, B. Corzilius, K. O. Tan, A. B. Barnes, E. Daviso, Y. Su, J. Herzfeld and R. G. Griffin, *J. Phys. Chem. B*, 2017, **121**, 4997-5006.
- 62 Y. Matsuki, T. Sugishita and T. Fujiwara, *J. Phys. Chem. C*, 2020, **124**, 18609-18614.